

**Figure 1.** Relative intensities as a function of  $\text{Ar}^+$  dose onto a Rh/TiO<sub>2</sub> thin-film system preheated to 775 K for 8 min in vacuum. The solid squares denote the H<sub>2</sub> TDS peak area after a 10 L exposure at 130 K, the solid triangles, the Ti/Rh AES ratio, and the solid circles, the Ti<sup>+</sup>/Rh<sup>+</sup> SSIMS ratio. The arrow marks the H<sub>2</sub> TDS area measured for the clean sample before heating to 775 K.

With increasing  $\text{Ar}^+$  dose, Figure 1 is characterized by a sharply declining Ti/Rh ratio and an increasing H<sub>2</sub> TDS peak area. For intermediate doses, these parameters remain relatively constant. As expected, the Ti/Rh ratio increases and the H<sub>2</sub> TDS area decreases for larger sputtering doses because the Rh layer is removed. Not shown in Figure 1 are the data for the O/Rh AES ratio, which follow the same trend as the Ti/Rh AES data. Clearly the ability to adsorb H<sub>2</sub> correlates with the amount of Ti and O present at the surface.

To explain these results, we proposed the following model. When the sample is heated, the surface of the Rh becomes more uniform and is partially encapsulated with a TiO<sub>x</sub> species. This species, which segregates to the Rh surface, probably migrates through defects in the Rh overlayer. It is a reduced oxide, as evidenced by the O/Ti AES ratio and Ti AES line shape. Further characterization of this Ti-O-Rh interface awaits XPS analysis. As the sample is depth profiled about 60% of the clean surface uptake capacity of H<sub>2</sub> is restored as the surface Ti is decreased. Since it is unlikely that implantation of Ti during the sputtering process could be responsible for the amounts of Ti present throughout the Rh overlayer, we suggest that some Ti diffuses into the Rh during annealing. Whether the Ti forms an alloy or is present in some other form is unclear from this work. The presence of Ti throughout the Rh layer coupled with the decrease in surface area expected from annealing the sample at 775 K for 8 min accounts for the inability of the sample to recover completely the original clean surface H<sub>2</sub> uptake.

Previously we reported that reduced titanium oxide interacts electronically with Pt to shift H<sub>2</sub> desorption to lower temperatures by 70 K.<sup>5</sup> This work was repeated for Rh under very carefully controlled conditions where neither Ti or O were present on the Rh surface (i.e., no encapsulation). As for Pt there was a significant shift of H<sub>2</sub> desorption peak to lower temperatures. Evidence of electronic interactions between metal and support has also been obtained using extended X-ray absorption fine structure (EXAFS).<sup>4</sup>

To summarize, the present work demonstrates that during heating to 775 K, Ti and O migrate through and segregate at the surface of thin Rh overlayers. As a result, sites for H<sub>2</sub> chemisorption are blocked. Previous work from this laboratory suggesting an electronic effect of TiO<sub>x</sub> on the ability of metals to chemisorb H<sub>2</sub> was verified for Rh. Taken together these results illustrate that SMSI effects can arise from a number of sources and that both encapsulation and electronic effects must be considered for the Rh/TiO<sub>2</sub> system.

Registry No. Rh, 7440-16-6; TiO<sub>2</sub>, 13463-67-7.

## Electron-Transfer Photochemistry of Allene-Iminium Salt Systems. Probes of Allene Cation Radical Structure by Theoretical and Chemical Techniques

Kenichi Somekawa,<sup>1</sup> Keith Haddaway, Patrick S. Mariano,\* and John A. Tossell

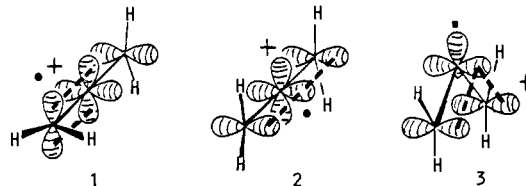
Department of Chemistry, University of Maryland  
College Park, Maryland 20742

Received October 12, 1983

During the past several years the area of electron-transfer photochemistry has received increasingly intense attention owing to the intriguing mechanistic and synthetic features of excited-state reactions initiated by single electron transfer (SET) between donor-acceptor pairs.<sup>2</sup> The reaction pathways promoted by this process are, for the most part, governed by secondary transformations of the initially formed radical ion species which compete with back electron transfer generating donors and acceptors in the ground state. Importantly, the results of photochemical processes initiated in this fashion contain an abundance of useful information about the solution-phase chemistry of ion radical species. Reaction processes promoted in this fashion have the potential for providing knowledge about regiochemical selectivities for nucleophilic and radical attack on delocalized radical cation systems.

Our previous studies with iminium salt systems<sup>2c,3</sup> have taken advantage of this unique feature of electron-transfer photochemistry to explore the solution-phase chemistry of radical cations generated from a variety of  $n$ -electron (alcohols, ethers) and  $\pi$ -electron (olefins, arenes, allylsilanes) donors. Recent efforts have focused on iminium salt-allene photoaddition reactions and have uncovered fundamentally important information about the structure and chemistry of allene-derived, cation radicals.<sup>4</sup>

A simple valence bond analysis of allene cation radicals suggests that several structures are possible for these systems, each having characteristic odd-electron and charge density profiles. The limiting structures are represented by what we shall designate as the linear-0°-twisted, linear-90°-twisted and bent-90°-twisted allene cation radicals, **1**, **2**, and **3**. Estimates of structure vs.



energy, charge density, and odd-electron density relationships for these systems were made by using ab initio MO calculations on the parent species,  $[\text{C}_3\text{H}_4]^+$ . The results of SCF level (UHF) calculations, employing minimal (STO-3G) and higher level (4-31G) basis sets<sup>5</sup> and the GAMESS program,<sup>6</sup> show that a linear-45°-twisted structure **4** represents the energy minimized geometry of  $[\text{C}_3\text{H}_4]^+$  and that this species has high positive charge density at the central carbon atom and large odd-electron density at the terminal carbons. Importantly, the energy vs. structure results are in accord with those obtained by MINDO/2<sup>7</sup> and MNDO-

(1) Current address: Department of Applied Chemistry, Kagoshima University, 1-21-40 Korimoto, Kagoshima, 890 Japan.

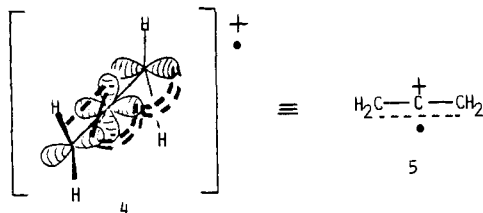
(2) (a) Davidson, R. S. In "Molecular Association"; Foster, R., Ed.; Academic Press: New York, 1975; Vol. 1, p 215. (b) Lablache-Combier, A. *Bull. Soc. Chim. Fr.* **1972**, *12*, 4791. (c) Mariano, P. S. *Acc. Chem. Res.* **1983**, *16*, 130; *Tetrahedron Suppl.*, in press.

(3) Mariano, P. S.; Stavinoha, J. L.; Bay, E. *Tetrahedron*, **1981**, *37*, 3385.

(4) (a) Additional information about the chemistry of allene cation radicals is found in earlier mass spectrometric<sup>6b</sup> and electrochemical studies<sup>6c</sup>. (b) Van Velzen, P. N. T.; Vanderhardt, W. J. *Org. Mass. Spectrosc.* **1981**, *16*, 237 and references therein. (c) Becker, J. Y.; Zinger, B. *Tetrahedron* **1982**, *38*, 1677 and references therein.

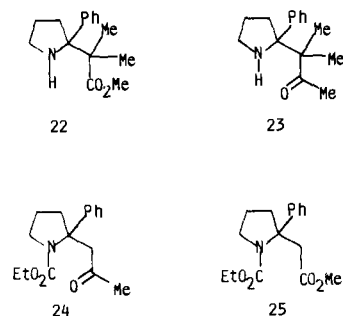
(5) Hehre, W. J.; Stewart, R. F.; Pople, J. A. *J. Chem. Phys.* **1969**, *51*, 2657.

(6) Dupuis, M.; Spangler, D.; Wendolowski J. *Nat. Resour. Comput. Chem. Software Cat.* **1980**, *1*, program No. QG01.



UHF<sup>8</sup> methods (which predict linear-52°-twisted and -45°-twisted minimum energy structures, respectively) and with analysis of vibrational fine structure in the PES spectrum of allene.<sup>9</sup> Interpreted more qualitatively, the results of the MO calculations substantiate the view that the minimum-energy structure for [C<sub>3</sub>H<sub>4</sub>]<sup>+</sup> represents a balance between the reduced, yet finite,  $\pi$ -bond order in the oxidized  $\pi$ -bond, the odd-electron delocalization into the unchanged  $\pi$ -bond, and the stabilization gained through  $\sigma_{\text{CH}}-\text{p}$  overlap (depicted in **4** by —, = = =, and — connections, respectively). Moreover, the results suggest that the resonance form depicted by **5** with high positive charge density at the central carbon best represents the allene cation radical.

The theoretical considerations presented above suggest that allene-derived, radical cations should participate in a variety of reactions including nucleophilic addition to the central carbon generating allyl radicals **6**, deprotonation at the terminal carbon providing propargylic radicals **7**, and coupling with radical trapping agents at the terminal carbon yielding vinyl cations **8** (Scheme I). Observations made in studies of electron-transfer-promoted photoaddition reactions of the parent and alkyl-substituted allenes **10–13** with 2-phenyl-1-pyrrolinium perchlorate (**9**) are consistent with this view of allene cation radical structure and solution-phase reactivity. Accordingly, irradiations (Corex) of methanolic solutions of **9** containing allenes **10–13** lead to modestly efficient production of the adducts shown in Scheme II. Product structures **14** are assigned on the basis of characteristic spectroscopic data and confirmed through use of degradative and relay transformations. For example, ozonolysis of the tetramethylallene adduct **14** provides the ester **22**, which is also formed by similar



reaction of the dimethylallene adduct **16**. Also, hydration of the acetylene **17** gives the same pyrrolidinylium ketone **23** as is obtained via hydrolysis of the enol ether **16**. Finally, ketal **18** and enol ether **15** are converted via hydrolysis and ozonolysis to their respective ketone and ester products, which, owing to their instability, are characterized as the carbamates **24** and **25**.

(7) Haselbach, E. *Chem. Phys. Lett.* **1970**, *7*, 428.

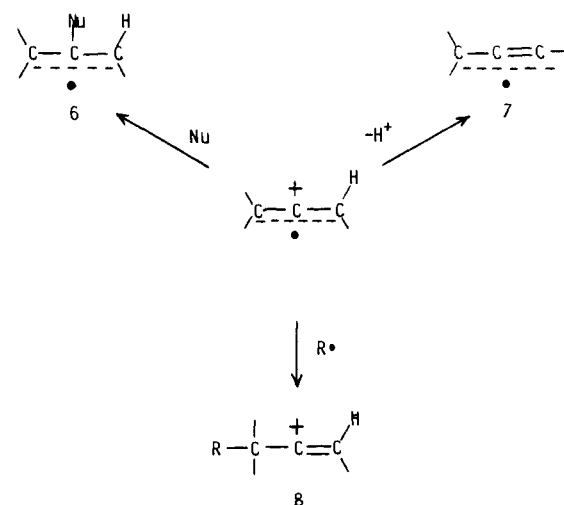
(8) (a) We thank Professor Nathan L. Bauld and Kurt Lorenz for making these results available to us. (b) The allene case thus differs from that of ethene where the MNDO results agreed well with those from experiments but the ab initio SCF results were substantially in error.<sup>8c</sup> (c) Bellvill, D. J.; Bauld, N. L. *J. Am. Chem. Soc.* **1982**, *104*, 294.

(9) (a) Baker, C.; Turner, D. W., *J. Chem. Soc., Chem. Commun.* **1967**, 480. (b) Koppel, H.; Cederbaum, L. S.; Domcke, W.; Shaik, S. S. *Angew. Chem., Int. Ed. Engl.* **1983**, *22*, 210.

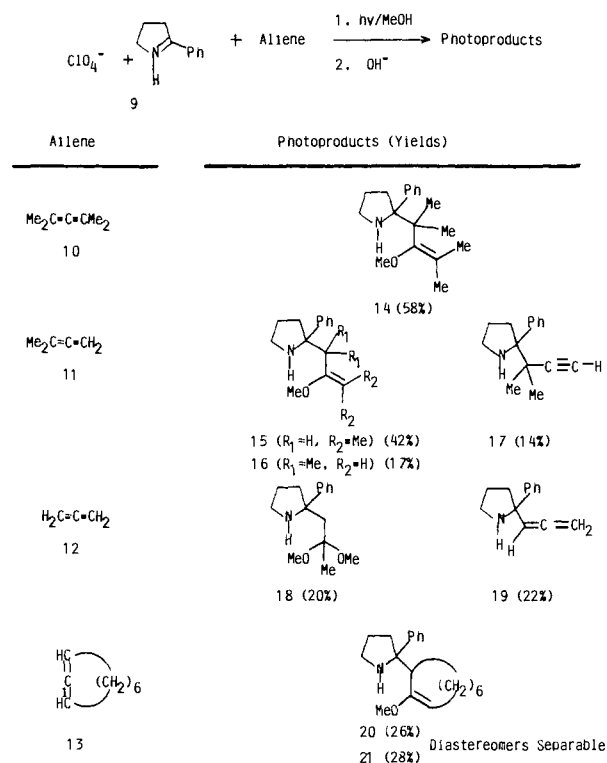
(10) Tetramethyl and 1,1-dimethylallene quench the fluorescence of pyrrolinium perchlorate **9** at near the diffusion-controlled rate ( $k_q = (3.8 \pm 0.2) \times 10^9 \text{ M}^{-1} \text{ s}^{-1}$  for **10** and  $(5.6 \pm 0.3) \times 10^9 \text{ M}^{-1} \text{ s}^{-1}$  for **11**, in CH<sub>3</sub>CN at 25 °C). Thus, under the preparative irradiation conditions in which allene concentrations are ca. 0.1 M efficient quenching and, thus, reaction of the pyrrolinium salt singlets should occur.

(11) All new compounds have satisfactory spectroscopic data and elemental compositions.

Scheme I



Scheme II



Two limiting mechanisms differing in the timing of methanol addition or deprotonation vs. radical coupling are possible for conversion of the initially formed radicals **26** + **27** to the photoadducts (Scheme III). Importantly, the observed regiochemical selectivities are consistent with either pathway since the theoretical picture developed earlier suggests that radical and nucleophile addition to **27** should occur at the terminal and central carbons, respectively. While results from our earlier studies with olefin-iminium salt systems<sup>2c,3,12</sup> would lead us to favor pathways in which allene radical cation transformations precede coupling to **26**, the current findings caution against such a conclusion. In particular, the observations that both regioisomeric enol ethers **15** and **16** and only the acetylene **17** are formed in photoaddition of **11** to **9** are also harmonious with routes in which radical coupling occurs prior to methanol addition or deprotonation. This is especially true in the case of coupling with the bulky and stabilized pyrrolidinylium radical where it is unlikely that the unsymmetric propargyl and allyl radicals **28** and **29** ( $R_1 = \text{CH}_3$ ;  $R_2 = \text{H}$ ) would

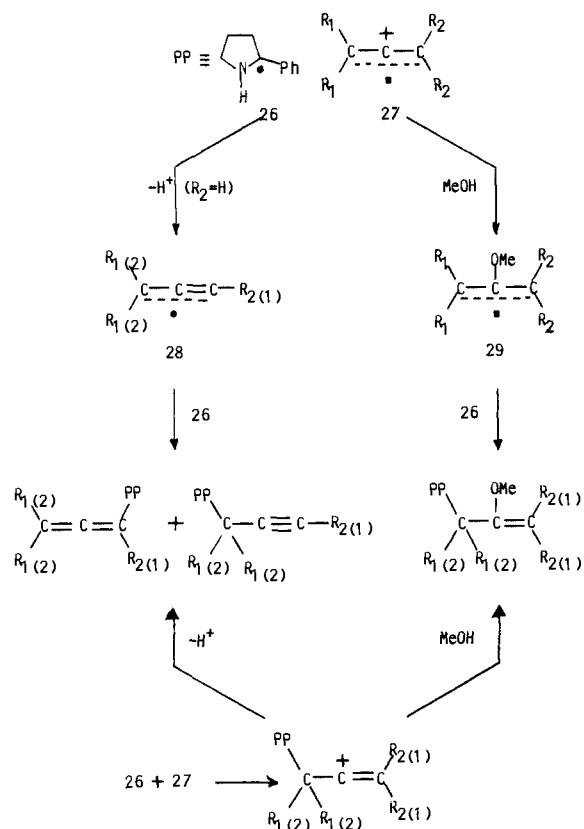
(12) Stavinoha, J. L.; Mariano, P. S. *J. Am. Chem. Soc.* **1981**, *103*, 3136.

**Table I.** Structure vs. Energy, Charge Density, and Odd-Electron Density Relationships for the Allene Cation Radical,  $[C_3H_4]^+$ , Calculated by SCF Methods with STO-3G and 4-31G Basis Sets

structure (symmetry)	energy relative to linear-45°-twist, kcal/mol		charge density <sup>c,d</sup>		odd-electron density <sup>d</sup>	
	STO-3G	4-31G	terminal C	central C	terminal C	central C
linear-0°-twist <sup>a</sup> ( $C_{2v}$ )	5.7	6.2	-0.33 -0.10	+0.12	0.07	0.25
linear-30°-twist ( $D_2$ )	1.2	0.9	-0.23	+0.13	0.34	0.27
linear-44.7°-twist <sup>b</sup> ( $D_2$ )	0.0	0.0	-0.25	+0.17	0.38	0.20
linear-60°-twist ( $D_2$ )	0.7	1.1	-0.30	+0.22	0.43	0.11
linear-90°-twist ( $D_{2h}$ )	2.0	4.3	-0.32	+0.28	0.50	0.00
bent-90°-twist <sup>a</sup> ( $C_{2v}$ )	16.7					

<sup>a</sup> All bond lengths are fully optimized. <sup>b</sup> The minimum-energy geometry represents a complete bond lengths and angles optimization. <sup>c</sup> For comparison, the calculated (STO-3G) values for the neutral allene, terminal and central carbon positive charge densities are -0.17 and +0.03, respectively. <sup>d</sup> Taken from SCF calculations using the 4-31G basis sets at STO-3G optimized geometries.

Scheme III



undergo partial or exclusive addition at the more highly substituted terminal positions (e.g., **16** and **17** formation).<sup>13</sup> On the other hand, this position would be favored for addition of **26** to the cation radical **27** ( $R_1 = CH_3$ ;  $R_2 = H$ ) where odd-electron and positive-charge density should be greatest in the alkyl-substituted  $\pi$ -bond.<sup>14,15</sup>

(13) (a) Trapping of unsymmetrically substituted allyl radicals should favor the less highly substituted carbons<sup>13b</sup> and of propargyl radicals should lead to both allene and acetylene products.<sup>13c</sup> (b) Ohga, K.; Mariano, P. S. *J. Am. Chem. Soc.* **1982**, *104*, 617 and references therein. (c) Fantazier, R. M.; Pontsma, M. L. *Ibid.* **1968**, *90*, 5490. Poutsma, M. L. *Tetrahedron Lett.* **1969**, 2925. Walling, C.; Heaton, L.; Tanner, D. D. *J. Am. Chem. Soc.* **1965**, *87*, 1715.

(14) The reduced degree of twisting for alkyl-substituted allenes postulated on the basis of the PES results<sup>9b</sup> is confirmed by our SCF (4-31G) calculations, which show a minimized geometry for the 1,1-dimethylallene cation radical having 1° twist angle, respective  $C_1$ - $C_2$  and  $C_2$ - $C_3$  bond lengths of 1.41 and 1.32 Å, and respective  $C_1$ ,  $C_2$ , and  $C_3$  odd-electron densities of 0.28, 0.36, and 0.05 and positive-charge densities of +0.2, +0.16, and -0.09.

(15) (a) An isolated, yet pertinent, observation of a similar nucleophilic addition to the central carbon of a highly phenyl-substituted allene cation radical is presented in a recent report by Johnson.<sup>15b</sup> (b) Klett, B.; Johnson, R. P. *Tetrahedron Lett.* **1983**, 1107.

Two final points are worthy of comment. Introduction of strain by incorporating the allene cation radical moiety into a medium-size ring (e.g., **13**) appears to have no effect upon the electronic properties of these systems. Thus, the bending force applied by the  $(CH_2)_6$  bridge in **13**<sup>+</sup> is energetically insufficient to cause adoption of a bent structure with high positive-charge density at the terminal carbons (see Table I). Also, generation of the ketal **18** from photoaddition of **12** to **9** occurs via an initially formed enol ether. The facility of this enol ether to ketal conversion compared to **14**-**16** can be attributed to the lack of  $\alpha$ -methyl substitution, which in the latter cases must render the ketal form excessively sterically congested.

The results summarized above demonstrate the unique potential of electron-transfer-initiated photochemical processes in probing the solution-phase chemistry of interesting charged radical systems. Continuing efforts in this area should clarify the mechanistic questions arising from the current results.

**Acknowledgment.** Financial support for this research was provided by grants from the NSF (CHE-09813 and CHE-21125). Helpful discussions with Nathan Bauld are also acknowledged.

### Nickel and Iron EXAFS of $F_{420}$ -Reducing Hydrogenase from *Methanobacterium thermoautotrophicum*<sup>†</sup>

Paul A. Lindahl,\* Nakao Kojima,\*<sup>‡</sup> Robert P. Hausinger,\* Judith A. Fox,\* Boon K. Teo,\*<sup>§</sup> Christopher T. Walsh,\* and William H. Orme-Johnson\*

Department of Chemistry  
Massachusetts Institute of Technology  
Cambridge, Massachusetts 02139

AT&T Bell Laboratories, Murray Hill, New Jersey 07974

Received December 19, 1983

*Methanobacterium thermoautotrophicum* produces two hydrogenases containing nickel and iron,<sup>1,2</sup> which are thought to catalyze the  $H_2$ -linked assimilation of  $CO_2$  required for energy-yielding methanogenesis<sup>3,4</sup> in this organism. We recently detected a nitrogen atom  $\geq 3.5$  Å from the nickel site in the  $F_{420}$  deazaflavin reducing hydrogenase<sup>1</sup> using electron spin echo spectroscopy.<sup>5</sup>

<sup>†</sup> Supported in part by NIH Grant GM 31574 and NSF Grant 8205764-PCM.

<sup>‡</sup> Present address: Institute of Applied biochemistry, Yagi Memorial Park, Gifu, Japan 505-01.

<sup>§</sup> AT&T Bell Laboratories, Murray Hill, New Jersey 07974.

(1) Jacobson, F. S.; Daniels, L.; Fox, J. A.; Walsh, C. T.; Orme-Johnson, W. H. *J. Biol. Chem.* **1982**, *257*, 3385-3388.

(2) Kojima, N.; Fox, J. A.; Hausinger, R. P.; Daniels, L.; Orme-Johnson, W. H.; Walsh, C. *Proc. Natl. Acad. Sci. U.S.A.* **1983**, *80*, 378-382.

(3) Daniels, L.; Fulton, G.; Spencer, R. W.; Orme-Johnson, W. H. *J. Bacteriol.* **1980**, *141*, 694-698.

(4) Spencer, R. W.; Daniels, L.; Fulton, G.; Orme-Johnson, W. H. *Biochemistry* **1980**, *19*, 3678-3683.